# Inhibition of TNF-α Improves the Bladder Dysfunction That Is Associated With Type 2 Diabetes

**Zongwei Wang,[1] Zhiyong Cheng,[2] Vivian Cristofaro,[3] Jijun Li,[1,4] Xingyuan Xiao,[1,5] Pablo Gomez,[6] Rongbin Ge,[1] Edward Gong,[6] Klemen Strle,[7] Maryrose P. Sullivan,[3] Rosalyn M. Adam,[6] Morris F. White,[2] and Aria F. Olumi[1]**

Diabetic bladder dysfunction (DBD) is common and affects 80% of diabetic patients. However, the molecular mechanisms underlying DBD remain elusive because of a lack of appropriate animal models. We demonstrate DBD in a mouse model that harbors hepatic-specific insulin receptor substrate 1 and 2 deletions (double knockout [DKO]), which develops type 2 diabetes. Bladders of DKO animals exhibited detrusor overactivity at an early stage: increased frequency of nonvoiding contractions during bladder filling, decreased voided volume, and dispersed urine spot patterns. In contrast, older animals with diabetes exhibited detrusor hypoactivity, findings consistent with clinical features of diabetes in humans. The tumor necrosis factor (TNF) superfamily genes were upregulated in DKO bladders. In particular, TNF-α was upregulated in serum and in bladder smooth muscle tissue. TNF-α augmented the contraction of primary cultured bladder smooth muscle cells through upregulating Rho kinase activity and phosphorylating myosin light chain. Systemic treatment of DKO animals with soluble TNF receptor 1 (TNFRI) prevented upregulation of Rho A signaling and reversed the bladder dysfunction, without affecting hyperglycemia. TNFRI combined with the antidiabetic agent, metformin, improved DBD beyond that achieved with metformin alone, suggesting that therapies targeting TNF-α may have utility in reversing the secondary urologic complications of type 2 diabetes. ***Diabetes*** **61:2134–2145, 2012**

Diabetes is reaching epidemic proportions and currently affects 8.3% of the U.S. population (1). Annually, 1.5 million new cases of diabetes are diagnosed. Type 2 diabetes accounts for 90% of newly diagnosed cases in the U.S. and is associated with chronic hyperglycemia. Deleterious complications of type 2 diabetes include heart disease, stroke, hypertension, retinopathy, neuropathy, nephropathy, and complications during pregnancy. From a urologic standpoint, patients with type 2 diabetes present with significant voiding complaints, recurrent urinary tract infections, and erectile dysfunction (2). Diabetic bladder dysfunction (DBD) is a common complication, affecting up to 80% of patients with diabetes (3), and causes a range of voiding and storage symptoms. Early DBD in compensated stages is frequently not recognized by patients or physicians due to its insidious development and inconspicuous symptoms; thus, by the time urologists are consulted, the DBD in diabetic patients has often reached an advanced stage in which the bladder is flaccid and poorly contractile (4).

DBD is traditionally described as a triad of decreased sensation, increased capacity, and poor emptying (5). However, recent clinical evidence indicates a more complex spectrum of bladder dysfunctions in patients with diabetes, including detrusor overactivity with or without urinary incontinence, impaired detrusor contractility, and detrusor areflexia (6). A multifactorial pathophysiology is supported by studies that have revealed disturbances of the bladder detrusor muscle, urethra, autonomic nerves, and urothelium (6,7).

Studies on streptozotocin (STZ)-induced type 1 diabetes suggest that DBD comprises two phases: a compensatory phase that occurs soon after the onset of diabetes and is characterized by bladder hypertrophy, remodeling, increased contractility, and associated neurogenic changes, followed by a decompensated phase that develops at later stages of diabetes featuring decreased peak voiding pressure (6,8,9). Despite significant recent advances in understanding the pathophysiology of DBD, the underlying molecular pathways that contribute to the secondary bladder complications of type 2 diabetes are poorly understood.

Patients are generally treated with hypoglycemic medications and muscarinic receptor antagonists to ameliorate the symptoms of overactive bladder. However, the underlying molecular alterations that can potentially be used for targeted therapies or identification of patients at risk for developing late stage are poorly understood. To investigate the molecular pathways associated with DBD, we used an animal model with conditional (cre-lox) hepatic double-knockout (DKO) of *Irs1* and *Irs2* genes (10,11). In this study, we show for the first time, that DKO mice developed bladder hyperactivity at age 6–12 weeks but showed bladder hypoactivity at age 16–20 weeks, a finding that parallels the variable and potentially temporal pathophysiologic alterations in bladder function in patients with type 2 diabetes. Furthermore, we discovered elevated levels of circulating and bladder tissue–associated TNF-α. We demonstrate that TNF-α directly stimulates bladder smooth muscle cell (BSMC) contraction, which can account for the bladder hyperactivity of the young DKO mice. We show that TNF-α activates Rho kinase (ROCK)–myosin light chain kinase (MLCK)–phosphorylating myosin light

From the [1]Department of Urology, Massachusetts General Hospital, Harvard Medical School, Boston, Massachusetts; the [2]Division of Endocrinology, Howard Hughes Medical Institute, Children's Hospital Boston, Harvard Medical School, Boston, Massachusetts; [3]Urology Research, Veterans Administration Boston Healthcare System, Harvard Medical School, Boston, Massachusetts; the [4]Department of Integrative Medicine, Shanghai Children's Medical Center, Shanghai Jiaotong University School of Medicine, Shanghai, China; the [5]Department of Urology, Wuhan Union Hospital, Huazhong University of Science and Technology, Wuhan, China; the [6]Urology Research Center, Children's Hospital Boston, Harvard Medical School, Boston, Massachusetts; and the [7]Department of Medicine, Division of Allergy/Immunology, Massachusetts General Hospital, Harvard Medical School, Boston, Massachusetts.

Corresponding author: Aria F. Olumi, olumi.aria@mgh.harvard.edu.

Received 29 December 2011 and accepted 14 March 2012.

DOI: 10.2337/db11-1763

This article contains Supplementary Data online at http://diabetes.diabetesjournals.org/lookup/suppl/doi:10.2337/db11-1763/-/DC1.

chain (pMLC) signaling, a pathway that when altered is known to cause bladder smooth muscle hypercontractility (12). More important, systemic inhibition of TNF-α–mediated signaling in mice reverses the DBD without affecting hyperglycemia in these animals. The combination of TNF-α inhibition and oral hypoglycemic therapy with metformin improves secondary urologic complications of DBD to a greater extent than that observed with metformin alone. Together, our findings suggest that targeted inhibition of the TNF-α pathway may have a role in treating DBD and reducing the burden of the secondary complications of type 2 diabetes.

## RESEARCH DESIGN AND METHODS

**Generation of DKO mice.** The floxed Irs1, Irs2 mice were generated as previously reported (10,11,13). To generate liver-specific knockout mice, floxed Irs1 and Irs2 mice were crossed with albumin-Cre mice (The Jackson Laboratory). The Irs1KO, Irs2KO and their corresponding control floxed mice were maintained on a C57/BL6 and 129Sv mixed genetic background. To avoid any potential obstructive effect of the prostate on the bladder, we used female DKO animals and their female littermates as control for these studies. All animal experiments were performed according to procedures approved by the Institutional Animal Care and Use Committee at Massachusetts General Hospital, Children's Hospital Boston.

**Cystometric evaluation of bladder function in vivo.** General anesthesia was induced by intraperitoneal injection of ketamine (100 mg/kg) and xylazine (10 mg/kg), the animal's bladder was surgically exposed, and a 25-gauge needle was introduced into the dome of the bladder and connected via a three-way adapter to a fluid-filled pressure line at one end and an injection pump (Harvard Apparatus) at the other. The pressure line was connected to a physiologic pressure transducer (MLT844 AD Instruments), and the bladder was filled with sterile saline at a constant rate (15 μL/min). The output signal was amplified and recorded using the Windaq system (Dataq Instruments) (14,15).

**Voided stain on paper (VSOP) analysis.** Mice were placed individually in metabolic cages with available food and water and allowed to adapt to their new environment for 24 h. Urine output was measured by evaluating the surface area of the stained VSOP paper (Bio-Rad) 3 h after the mice were placed in the metabolic cages. Collected papers were imaged under ultraviolet light to visualize the urine and analyzed by using the edge-detection function of ImageJ software (National Institutes of Health [NIH]) to identify the surface area of individual voided urine spots. The volumes of individual voids were calculated based on a calibration curve relating surface area to fluid drops of known volume (14,15).

**Assessment of bladder smooth muscle contractility.** Full-thickness longitudinal detrusor muscle strips (0.7 to 1 × 3.5 to 5 mm) were prepared and transferred to 5 mL tissue baths containing Kreb's solution bubbled with a mixture of oxygen (95%) and carbon dioxide (5%). One end of each strip of tissue was tied by silk suture to a fixed hook and the other to a force transducer. Bladder tissue was stretched to a passive tension of 0.5 g and allowed to equilibrate for 60 min before experiments were performed. The frequency and amplitude of spontaneous activity was determined over a 5-min interval after the equilibration period. In addition, the contractile response to stimulation of bladder tissue by potassium chloride (KCl) (120 mmol/L) and electrical field stimulation (EFS; 2, 4, 8, 16, 32, 64 Hz; 40 V; 0.5 ms pulse duration for 10 s) was measured. The dose-response curve for carbachol was generated by adding cumulative concentrations of the agonist ($10^{-9}$ to $10^{-5}$ mol/L) to the bath. Isometric force was continuously recorded with a computerized data acquisition program at a sampling rate of 20 Hz. At the end of experiments, the weight, length, and width of each strip was measured to normalize the force data (16).

**Affymetrix gene array analysis.** The Affymetrix GeneChip analysis was performed as previously described (10,11). Briefly, total RNA was extracted from bladder smooth muscle tissues using the RNeasy Mini Kit (Qiagen, Valencia, CA) according to the manufacturer's instructions. Microarray analysis was conducted by the Harvard Partners HealthCare Center for Personalized Genetic Medicine Microarray Facility using 15 μg RNA from each sample, with each group in triplicate. Gene expression was analyzed by using Mouse Genome 430 2.0 array system (Affymetrix). The Database for Annotation, Visualization and Integrated Discovery (DAVID Bioinformatics Resources 6.7, NIH) was used to categorize the most significantly changed genes (upregulated 1.5-fold or more relative to age-matched control) by biologic functions or disease processes.

**BSMC isolation, culture, and transfection.** Rat BSMCs were isolated from 1-week-old Sprague-Dawley female rats, as described previously (17). The cell pellet was resuspended in medium 199 (Gibco) and used for experiments up to passage 3. For gene suppression experiments, BSMCs were transfected with small interfering (si)RNA at 40% confluency using siIMPORTER transfection reagent (Millipore), according to the manufacturer's instructions.

**Collagen gel retraction assay.** Collagen lattice was carefully prepared in 24-well plate by collagen type 1 from rat tail (Sigma) (18). A total of 25,000 BSMCs were layered onto each collagen lattice and left to settle for 2 h at 37°C. To allow contraction, each collagen lattice was detached from the bottom of the well with a small spatula and left overnight at 37°C. Contraction was stopped by fixing the lattices in PBS-4% paraformaldehyde, and the plate was photographed. Image analyses of the gel area were performed by using ImageJ software (NIH).

**Western blot analysis.** Immunoblotting was performed as previously described (19). To stimulate the phosphorylation of MLC, bladder smooth muscle tissues were treated with 80 mmol/L KCl for 15 s and then quickly frozen in liquid nitrogen (20), and cultured BSMCs were treated with 80 mmol/L KCl for 5 min. Total protein was quickly extracted on ice (21), and the protein extracts were subjected to SDS-PAGE and blotted. Membranes were probed with target antibodies.

**Immunostaining.** As described previously (22), sections (5 μm) from paraffin-embedded tissue underwent antigen retrieval with proteinase K (Dako) and were incubated with primary and secondary antibody. Cells grown on glass coverslips were fixed in 4% paraformaldehyde, permeabilized with 0.2% Triton X-100/PBS, and stained with antibodies (23).

**Evaluation of the activity of ROCK1 or ROCK2 in cell lysates.** Activation of ROCK1 or ROCK2 was evaluated by immunoprecipitating ROCK1 or ROCK2, followed by an in vitro kinase activity assay (24). Cells were lysed using cell lysis buffer (Cell Signaling), and cleared lysates were incubated for 1 h at 4°C with 2 μg isotype control IgG, anti-ROCK1, or anti-ROCK2 (Santa Cruz). The mixture was incubated with protein A/G agarose beads at 4°C overnight. The beads were pelleted, washed, and incubated for 30 min at 30°C with kinase reaction buffer containing 200 μmol/L ATP (Cell Signaling) and 0.5 μg purified myosin phosphatase target subunit 1 (MYPT-1; Millipore), a ROCK-specific substrate. The reaction was terminated by boiling the samples in SDS. The amount of phosphorylated MYPT-1 or immunoprecipitated ROCK1 or ROCK2 was examined using immunoblot.

**ROCK activity assay in animal tissue.** ROCK enzymatic activity was determined with a commercially available Cyclex Rho kinase Assay Kit-96 (MBL International) (25).

**Cytokine assay.** Cytokine productions were analyzed with a Milliplex Map Kit for mouse cytokine assay (Millipore) according to the manufacturer's instructions, which allowed the simultaneous quantification of the following mouse cytokines: granulocyte-macrophage colony-stimulating factor, interferon-γ, interleukin (IL)-1β, IL-2, IL-4, IL-5, IL-6, IL-10, IL-12(p70), and TNF-α. In anti-TNF receptor (TNFR) treatment experiments, the level of TNF-α in serum was determined using commercial mouse TNF-α ELISA Kit (eBioscience) according to the manufacturer's protocol.

**Blood glucose analysis.** Blood glucose levels were measured using a portable glucometer (Bayer). For glucose tolerance tests (GTT), mice were fasted overnight and injected intraperitoneally with D-glucose (2 g/kg body weight), and blood glucose levels were measured at indicated time points, as previously described (10).

## RESULTS

**Temporal alteration of DKO bladder function.** We first evaluated whether the DKO mice exhibit alterations in bladder function and found that DKO mice exhibited significantly higher amplitudes of spontaneous activity at age 6 and 12 weeks relative to age-matched controls (Fig. 1*A* and *B*). In contrast, 16- and 20-week-old DKO mice demonstrated lower amplitudes of spontaneous activity than age-matched controls (Fig. 1*A* and *B*). Meanwhile, the frequency of spontaneous activity in the bladders did not vary (Fig. 1*C*). The contractile responses of bladder tissue to KCl (120 mmol/L; Fig. 1*D*) and carbachol stimulation ($10^{-9}$ to ~$10^{-5}$ mol/L; Fig. 1*E* and *F*) were significantly greater in young DKO mice (age 6–12 weeks), but significantly diminished in 20-week-old DKO mice compared with age-matched control animals. However, the response to carbachol stimulation in control mice was not different among age groups (Fig. 1*F*), which ruled out the possibility of age-dependent changes in cholinergic receptor sensitivity. We further induced neurogenically mediated bladder contractions by EFS (26,27) and

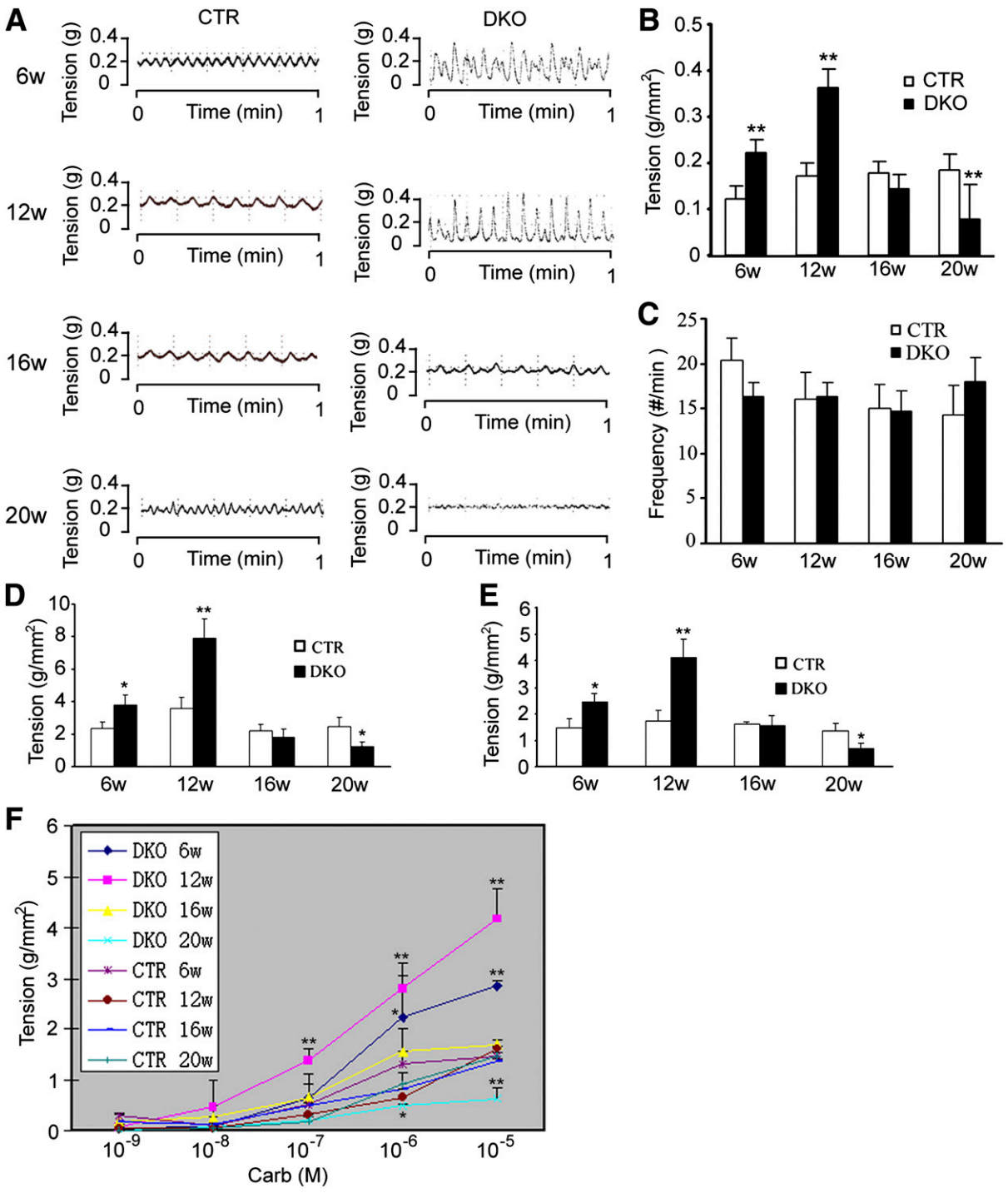


**FIG. 1. DKO mice exhibit increased spontaneous and stimulated bladder contractions early in life and decreased contractions later in life. *A*: Representative spontaneous contractions of bladder strips in floxed control (CTR) and liver-specific Irs1/Irs2 DKO mice. Quantification of the amplitude (*B*) and frequency (*C*) of spontaneous contraction. *D*: Bladder smooth muscle contraction induced by KCl (120 mmol/L) stimulation in DKO and CTR mice. Bladder smooth muscle contraction induced by carbachol (Carb) stimulation at $10^{-5}$ mol/L (*E*) and $10^{-9}$ to ~$10^{-5}$ mol/L (*F*). The tension data were obtained from eight strips from four animals in each group and normalized by the length, width, and weight of muscle strips. Bladder tissue was stretched to a passive tension of 0.5 g and allowed to equilibrate for 45 to ~60 min before experiments were performed. Isometric force was continuously recorded with a computerized data acquisition program at a sampling rate of 20 Hz. CTR indicates the littermate combined floxed *Irs1* and *Irs2* gene control animal. Data are representative of at least three different experiments and are expressed as the means ± SEM, by unpaired Student *t* test. *$P < 0.05$ and **$P < 0.01$ compared with age-matched control group. w, weeks.**

found that the contractile response to EFS was augmented in bladder tissue of 6- and 12-week-old DKO mice but diminished in older mice at ages 16 and 20 weeks (Supplementary Table 1).

**DKO mice showed an abnormal urine voiding pattern.** To gain further insight into the development of bladder dysfunction associated with type 2 diabetes, we evaluated the urinary voiding patterns in the DKO mice in vivo by

performing cystometry and VSOP analysis. During cystometry, the voiding pattern in DKO mice was markedly altered. Although the micturition frequency did not change significantly (Fig. 2*A* and *B*), 12-week-old DKO animals exhibited clear signs of bladder overactivity, characterized by increased frequency of nonvoiding contractions and significantly reduced voided volumes (Fig. 2*C* and *E*). For 20-week-old DKO animals, however, the amplitude of

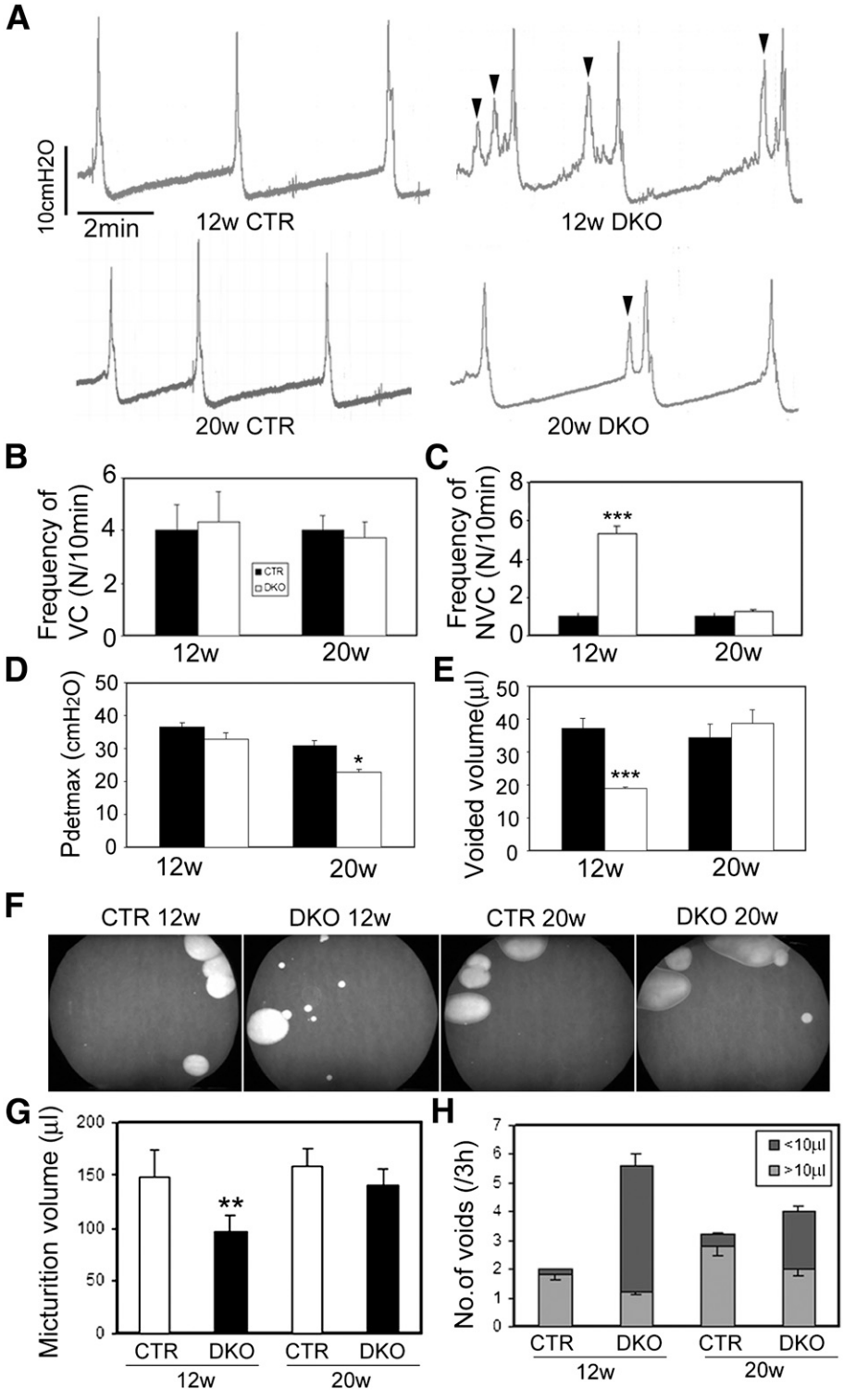


**FIG. 2. DKO animals exhibit abnormal voiding pattern. *A*: Original cystometric recordings in control (CTR) and DKO mice at the age of 12 and 20 weeks (w). Arrowheads reflect abnormal bladder contractions not associated with urination. Evaluation of urodynamic parameters: frequency of voiding contractions (VC) (*B*), frequency of nonvoiding contractions (NVC) (*C*), amplitude of the detrusor contraction during voiding ($P_{detmax}$) (*D*), and voided volumes (*E*) ($n$ = 6 for DKO; $n$ = 5 for CTR). *F*: Representative spontaneous micturition pattern of unrestrained animals. *G*: Micturition volume. *H*: The frequency of smaller volume voids (<10 μL). The slope of the calibration curve ($cm^2$)/volume (μL) was 0.14 (1 $cm^2$ of area corresponds to 7.14 μL volume; $n$ = 6 mice for each group). Data are representative of at least three different experiments and are expressed as the means ± SEM, by unpaired Student $t$ test. *$P$ < 0.05, **$P$ < 0.01, and ***$P$ < 0.001 compared with age-matched control group.**

bladder contractions during voiding was lower than for age-matched controls (Fig. 2*D*). In comparison, we found a normal pattern of bladder contraction and voiding in 12- or 20-week-old control mice (Fig. 2*A*), which is in line with other reports (14,15).

In the VSOP test, freely moving floxed control animals showed a normal voiding pattern: voiding occurred around the edge of the cage, and few voided urine spots appeared in the middle of the cage (Fig. 2*F*) (15). However, the voided stains for the DKO mice were much more dispersed, with multiple urine spots away from the edge, suggesting an abnormal voiding pattern (15) (Fig. 2*F*). Notably, the micturition volumes were lower and the frequency of small volume voids (<10 μL) was higher in DKO mice than in age-matched controls, especially for 12-week-old DKO mice ($P < 0.01$) (Fig. 2*G* and *H*). Taking the cystometric and VSOP data together, DKO animals developed abnormal voiding behavior with increased frequency of nonvoiding contractions and significantly reduced voided volumes at the age 12 weeks, which exhibited clear signs of bladder overactivity. For 20-week-old DKO animals, the low amplitude of bladder contractions in tissue and cystometric tests demonstrated decreased contractility at this stage.

**Characterization of systemic and local inflammatory mediators in bladder tissue of DKO animals.** Using the Affymetrix GeneChips, we compared 45,000 genes in bladder smooth muscle between the diabetic DKO and control animals. We found 30 genes that were upregulated 1.5-fold or greater in 12-week-old DKO animals relative

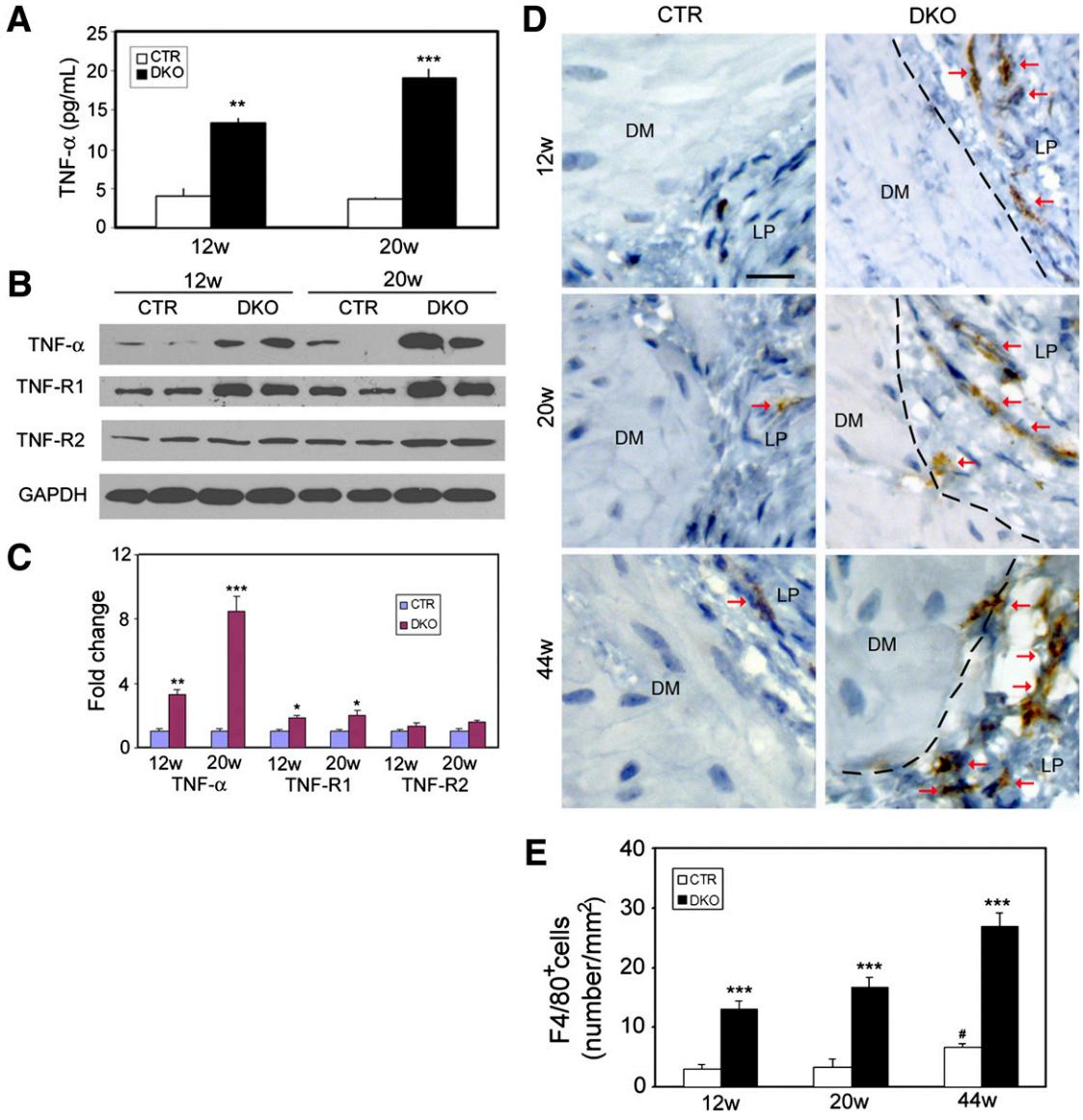


**FIG. 3. Increased inflammatory mediators in DKO mice. *A*: Serum soluble TNF-α level. *B*: Representative immunoblot of three different experiments of TNF-α and TNFR1 protein levels. C: Quantification of immunoblot protein expression by normalization to glyceraldehyde-3-phosphate dehydrogenase (GAPDH). *D*: Representative immunostaining for macrophages (*arrows pointed*). DM, detrusor muscle; LP, lamina propria; w, weeks. Original magnification ×400. Scale bar: 20 μm. *E*: Quantification of F4/80$^+$ macrophages in bladder tissue. The results in bar graphs are presented as mean ± SEM, $n = 5$, by unpaired Student $t$ test (*A* and *C*) or 1-way ANOVA (*E*). *$P < 0.05$, **$P < 0.01$, and ***$P < 0.001$ compared with age-matched control group; #$P < 0.05$ compared with 12-week-old control. (A high-quality digital representation of this figure is available in the online issue.)**

to age-matched controls (Supplementary Table 2). Of these, 20 genes were inflammatory mediator genes that belonged to the TNF family and were also persistently elevated in 20-week-old mice. Because inflammation is known to play an important role in the pathogenesis of diabetic organ damage (28), we wished to determine whether TNF-α plays any role in DBD. We found that the serum level of TNF-α was elevated in 12- and 20-week-old DKO animals compared with age-matched controls (Fig. 3*A*), although the protein levels of 10 cytokines in urine and homogenized bladder tissue were below the limit of detection by the Milliplex kit assay. Western blot analysis also showed that TNF-α and TNFR1 were significantly upregulated in DKO bladder tissue, whereas TNFR2 expression did not change (Fig. 3*B* and *C*).

Immunohistochemistry staining for the macrophage-specific marker F4/80 further showed that F4/80$^+$ macrophages significantly increased in DKO animal bladders in an age-dependent manner (Fig. 3*D* and *E*). Interestingly, immunoreactivity for macrophages localized in the lamina propria (i.e., junction between smooth muscle and epithelial layers; Fig. 3*D*). Together, these data suggest that circulating and bladder-localized inflammatory mediators are upregulated in DKO animals.

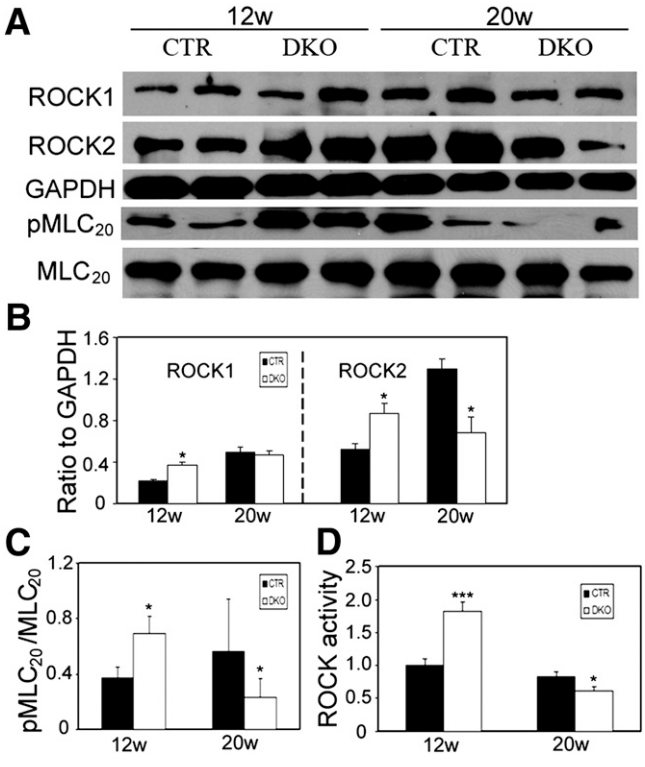


**FIG. 4. Expression of ROCK and $MLC_{20}$ proteins and activity of Rho kinase is associated with contractility in DKO bladders. *A*: Representative immunoblot analysis in bladder smooth muscle extracts. Glyceraldehyde-3-phosphate dehydrogenase (GAPDH) was used as a loading control. *B* and *C*: Densitometric analyses of immunoblot. The level of ROCK1 and ROCK2 was normalized to GAPDH, and the level of $pMLC_{20}$ was expressed as a percentage of total $MLC_{20}$ protein levels. *D*: ROCK activity of bladder smooth muscle homogenates, which was expressed as optical density (OD) and normalized to control (CTR) group. Data were from three independent experiments and presented as mean ± SEM, by Student *t* test. *$P < 0.05$ and ***$P < 0.001$ compared with age-matched control group. w, weeks.**

**Rho kinase activity is altered in DKO bladder smooth muscle.** Microarray analysis of bladders of 12-week-old DKO animals demonstrated increased expression in the genes encoding ATPase, Rho GTPase, and Rho kinase, which are known as important regulators of cellular metabolism and contractility, but decreased expression in 20-week-old DKO mice (Supplementary Table 2). Therefore, we next evaluated Rho kinase protein expression in bladder smooth muscle tissue. Western blot analysis showed that both ROCK isoforms, ROCK1 and ROCK2, were significantly upregulated in 12-week-old mice. In 20-week-old DKO animals, ROCK2 was significantly downregulated compared with age-matched controls (Fig. 4*A* and *B*). We measured ROCK activity in bladder homogenates and further observed that the kinase activity was elevated in 12-week-old but reduced in 20-week-old DKO animals (Fig. 4*D*). Consistent with these changes, the level of phosphorylated $MLC_{20}$ ($pMLC_{20}$) was increased in 12-week-old DKO mice but decreased in 20-week-old DKO mice (Fig. 4*C*). These findings suggest that the temporal changes in expression levels of ROCK1 and ROCK2 correlated with the hyperactivity and hypoactivity states of bladders in young and old DKO animals, respectively.

**TNF-α directly promotes BSMC contraction.** We next addressed whether TNF-α directly contributed to the bladder dysfunction. Growing BSMCs from DKO and control mice in primary tissue cultures was challenging because we could not obtain an adequate number of cells for in vitro experiments. Therefore, we used primary rat BSMCs, which we were able to passage in culture. Administration of 1–30 ng/mL TNF-α for 2.5 h dramatically promoted the contraction of BSMC in a dose-dependent manner (Fig. 5*A*) and upregulated $pMLC_{20}$ and the phosphorylation of calmodulin (pCalm; Fig. 5*B* and *C*). Interestingly, high glucose (22 mmol/L) treatment alone, even for 24 h, did not promote cellular contraction (Fig. 5*D*). Immunostaining with $pMLC_{20}$ antibody further confirmed that TNF-α stimulated the phosphorylation of $MLC_{20}$ (Supplementary Fig. 1*A* and *B*). However, pretreatment of cells with MLCK inhibitor P18 or ROCK inhibitors (Y27632 and Fasudil) for 30 min before administration of TNF-α significantly inhibited the ability of TNF-α to promote cell contraction (Fig. 5*D* and *E*) and suppressed the level of $pMLC_{20}$ (Supplementary Fig. 1*C* and *D*). Our results suggest that TNF-α may augment cellular contraction through activation of the calcium-dependent Rho kinase–MLCK–pMLC pathway.

**ROCK1 and ROCK2 mediate TNF-α–induced MLC phosphorylation.** To further investigate the signaling pathway affected by TNF-α in BSMCs, we immunoprecipitated ROCK1 and ROCK2 from BSMCs and evaluated their activity through in vitro kinase activity assay using purified MYPT-1 as a substrate. Antibodies against ROCK1 or ROCK2 efficiently immunoprecipitated their presumed target (Fig. 6*A*). ROCK1 and ROCK2 were able to phosphorylate MYPT-1 in the kinase assay, and this phosphorylation could be abolished by Y27632, the Rho kinase inhibitor (Fig. 6*B*). Compared with untreated cells, the activity of ROCK1 and ROCK2 was increased by TNF-α stimulation between 5 min and 3 h, indicating that both ROCK isoforms are activated by TNF-α (Fig. 6*C* and *D*). However, downregulating of ROCK1 and ROCK2 with ROCK1 siRNA or ROCK2 siRNA alone, or combined, prevented the TNF-α stimulated increase in phosphorylation of $MLC_{20}$, especially at 6 h (Fig. 6*E–I*). Together, these data suggest that ROCK1 or ROCK2 is necessary to induce $MLC_{20}$ phosphorylation in response to TNF-α stimulation.

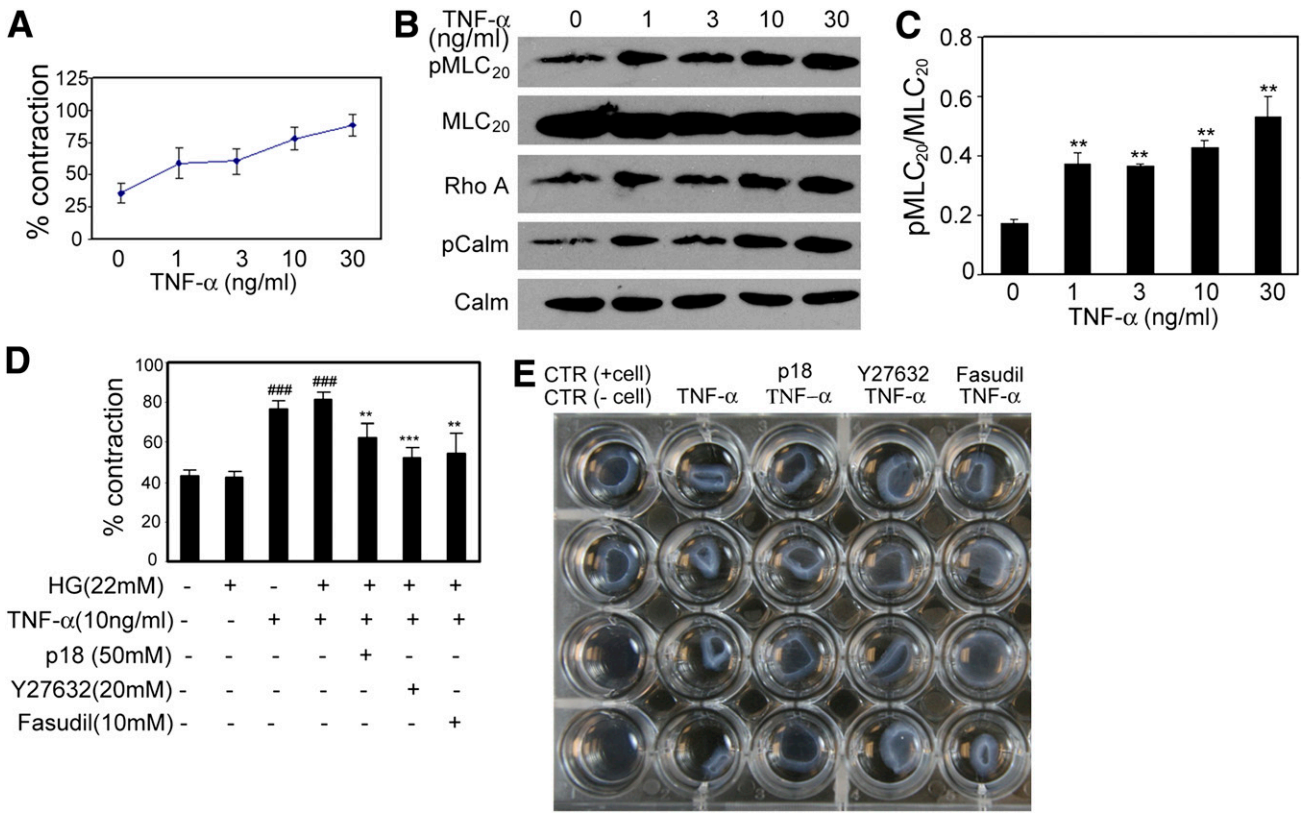


**FIG. 5. TNF-α promotes BSMC contraction. *A*: TNF-α promoted contraction of BSMC in a dose-dependent manner. *B*: Representative of three independent immunoblots of BSMCs stimulated with 1–30 ng/mL TNF-α. *C*: Quantification of $MLC_{20}$ phosphorylation. *D*: The effect of high glucose (HG, 22 mmol/L D-glucose, Invitrogen), MLCK inhibitor peptide 18 (p18, Tocris Bioscience), ROCK inhibitor Y27632 (Enzo Life Sciences), and Fasudil (Tocris Bioscience) on TNF-α–induced cell contraction. *E*: Representative cell contraction image of three independent experiments. The cell contraction was detected after 2.5 h treatment with 10 ng/mL TNF-α, pretreated with inhibitors for 30 min or pretreated with HG for 24 h. CTR, untreated control; Calm: total calmodulin; pCalm, phospho calmodulin. Cell contraction was determined in triplicate or quadruplicate and expressed as the percentage of contraction, which was quantitated as the percentage of lattice size diminution relative to the area of the well. Data are representative of three different experiments and are expressed as the means ± SEM, by Student *t* test (*C*) or one-way ANOVA (*D*). ###$P < 0.001$ compared with untreated group; **$P < 0.01$ and ***$P < 0.001$ compared with TNF-α–treated group. (A high-quality color representation of this figure is available in the online issue.)**

**Neutralizing TNF-α improves bladder function in DKO animals without effects on hyperglycemia.** On the basis of these findings, we wished to investigate whether anti–TNF-α treatment would be a target for treating diabetes-related bladder dysfunction. Systemic inhibition of TNF-α activity with soluble TNFR1 (TNFRI) in DKO mice resulted in a significantly decreased frequency of nonvoiding contractions and an increase in voided volumes compared with untreated DKO mice (Fig. 7*A*, *C*, and *D*), although the frequency of micturition and amplitude of voiding contractions were not changed significantly ($P > 0.05$, Fig. 7*B* and *E*). Administration of TNFRI also improved the voiding behavior of freely moving animals, as reflected by a more controlled and organized voiding pattern, less dispersed urine spots, larger micturition volume, and lower frequency of small volume voids (<10 μL; Fig. 7*F–H*).

When determining whether the observed bladder dysfunction was associated with the concentration of circulating TNF-α, we found the serum TNF-α level in DKO mice was significantly reduced after 6 weeks of treatment and approached a level similar to that of the floxed control animals (Fig. 7*I*). In addition, the elevated ROCK activity as well as ROCK1 and ROCK2 protein expression in DKO bladder smooth muscle homogenates were suppressed (Fig. 7*J*). Consistent with these effects, anti–TNF-α treatment not only suppressed the TNF-α expression in bladder smooth muscle but also lowered the expression of $pMLC_{20}$, pCalm, ROCK1, ROCK2, and Rho A (Fig. 7*K*). Meanwhile, anti–TNF-α treatment alone did not lower the blood glucose level in DKO mice (Fig. 7*L–N*). However, administration of the antidiabetes drug, metformin, alone or combined with TNFRI, significantly suppressed the blood glucose level after 6 weeks of treatment as assessed by the GTT assay (Fig. 8*A–C*). More important, TNFRI and metformin synergistically decreased the serum TNF-α level (Fig. 8*D*) and improved the bladder dysfunction after 6 weeks of treatment, as shown by a significant decrease in frequency of nonvoiding contractions during urodynamic testing (Fig. 8*E*) and a decreased number of small-volume voids in VSOP analysis (Fig. 8*F*). Our results demonstrate the significance of targeted molecular treatment for correcting or preventing the secondary complications of diabetes.

## DISCUSSION

DBD affects 80% of diabetic patients; however, the molecular mechanisms underlying DBD remain elusive due to the lack of appropriate animal models. Bladder contraction is mediated by cholinergic and purinergic pathways (26,29). Here, we found phenotypic differences in the behavior of isolated bladder strips in DKO animals. In particular, the spontaneous activity in early-stage DKO mice (age 6 and 12

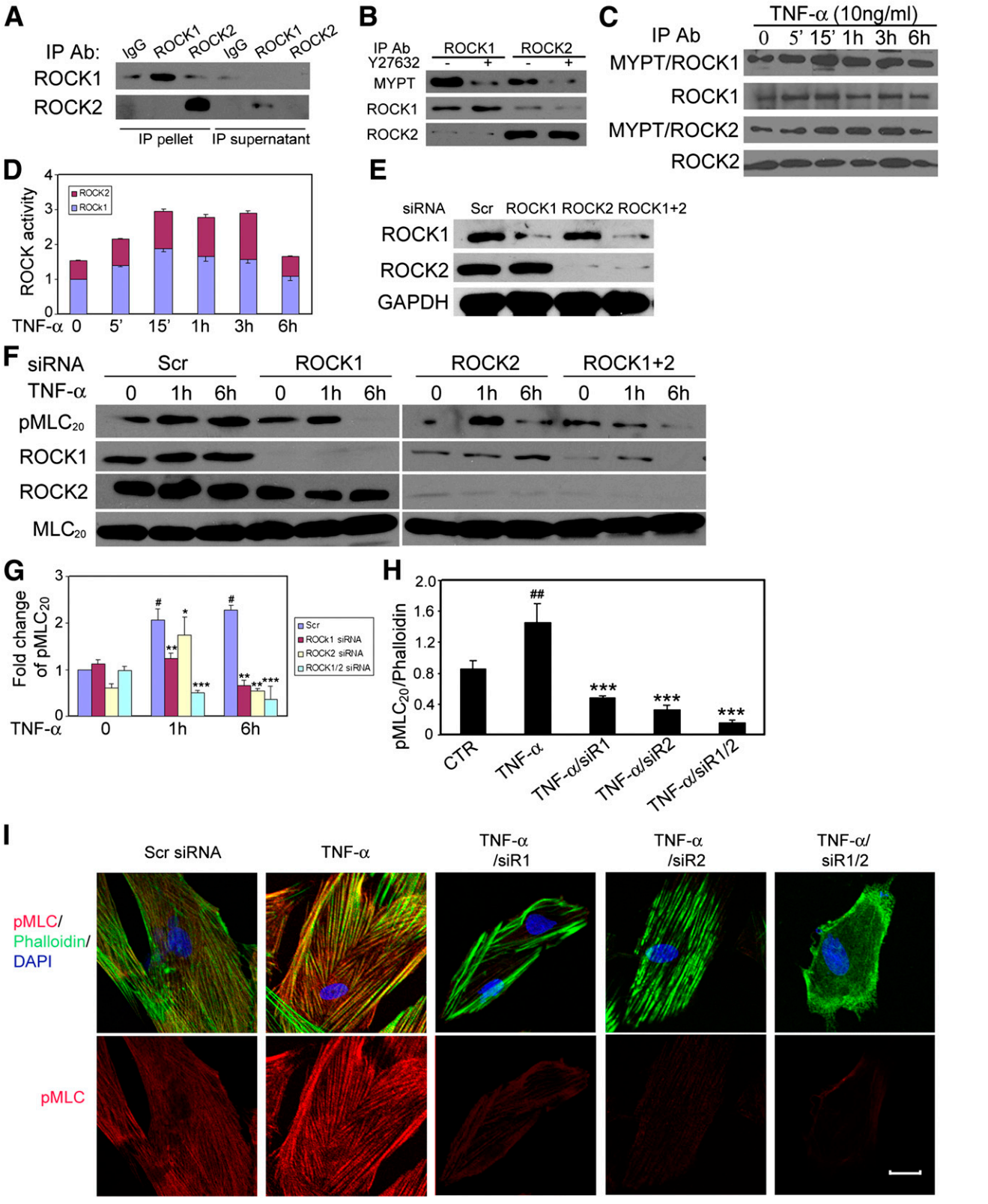


**FIG. 6. ROCK1 and ROCK2 regulate TNF-α–induced $MLC_{20}$ phosphorylation. *A*: Isoform-specific ROCK immunoprecipitation. *B*: Kinase activity assay. *C*: Determination of ROCK activation in BSMCs after TNF-α stimulation. *D*: Quantification of ROCK activity: The ROCK1 activity in untreated control cells was defined as 1, and the relative amount of ROCK1 and ROCK2 activity was presented. *E–G*: Augmentation of ROCK1 or ROCK2 by TNF-α expression was inhibited by suppression of ROCK1 or ROCK2 using siRNA. BSMCs were transfected with scrambled (Scr) or ROCK1/ROCK2-targeted siRNA for 48 h, followed by TNF-α stimulation for 1 or 6 h, and protein expression of ROCK1 or ROCK2 (*E*), or the level of $pMLC_{20}/MLC_{20}$ (*F*) was examined by immunoblot and quantified (*G*). *H*: Quantification of $pMLC_{20}$ expression in immunostained BSMCs. The phosphorylation of $MLC_{20}$ was quantified and normalized as the ratio of $pMLC_{20}$ relative to phalloidin. Data are expressed as mean ± SEM by two-way ANOVA (*G*) or one-way ANOVA (*H*). #$P < 0.05$ and ##$P < 0.01$ compared with scrambled group at 0 h; *$P < 0.05$, **$P < 0.01$, and ***$P < 0.001$ compared with TNF-α–treated scrambled group, respectively. *I*: Representative immunofluorescence microscopy of BSMCs of three different experiments. Scale bar: 20 μm. (A high-quality digital representation of this figure is available in the online issue.)**

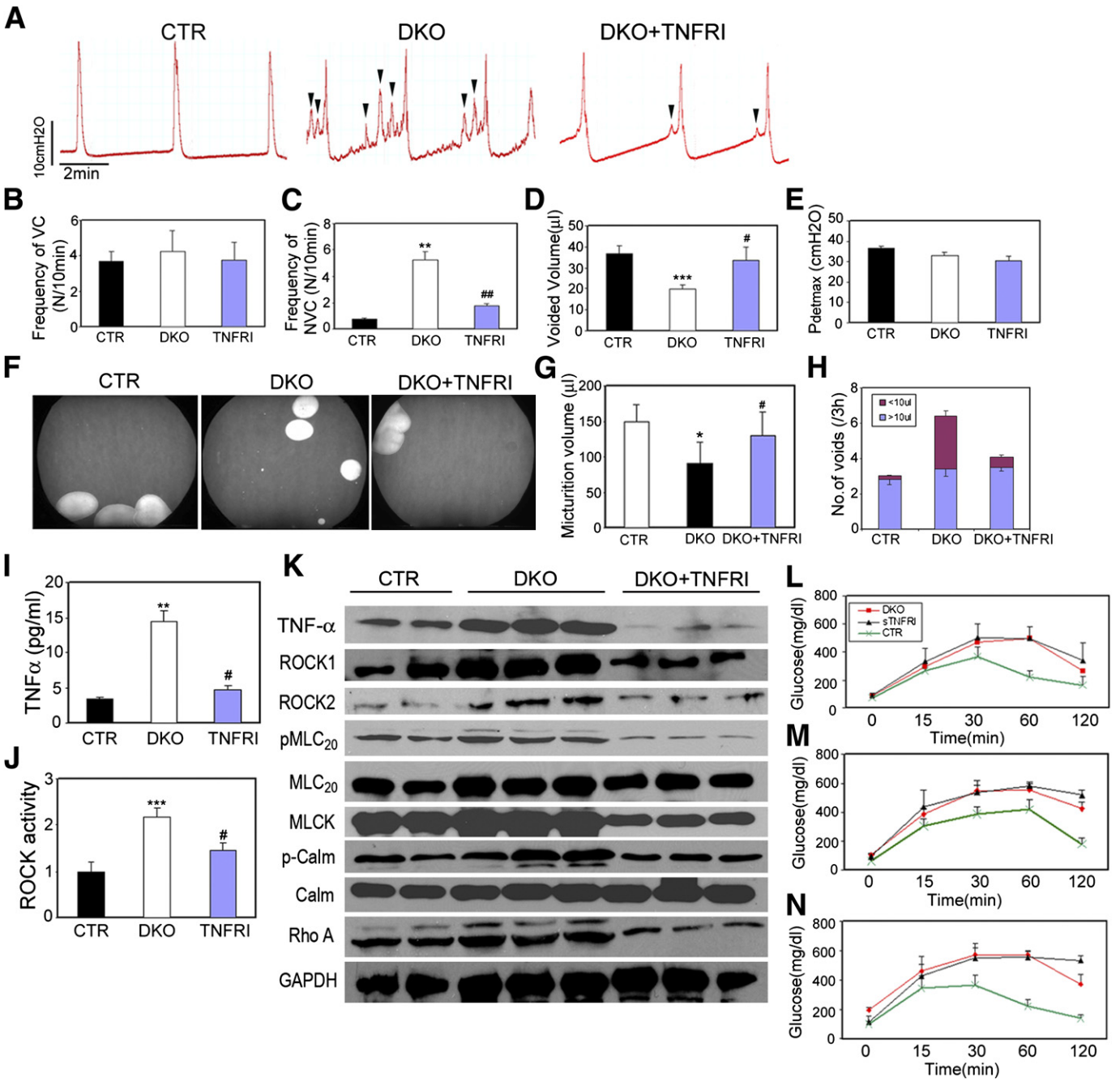


**FIG. 7. TNFRI treatment reversed bladder dysfunction of 12-week-old DKO mice. Six-week-old animals were intraperitoneally injected with soluble TNFR1 (TNFRI, 2 mg/kg, PEG-TNFRI, Amgen), twice per week, or saline solution for controls. Blood GTT was performed before the treatment and after 3- and 6-week treatment. After 6 weeks of treatment, half of the animals were evaluated by VSOP analysis and cystometry. Remaining mice were killed and bladders were retrieved for protein extraction. *A*: Representative cystometry recordings. Arrowheads represent abnormal nonvoiding bladder contractions. *B*: Frequency of voiding contractions (VC). *C*: Frequency of nonvoiding contractions (NVC). *D*: Volume of voids. *E*: Detrusor pressure during voiding contractions ($P_{detmax}$). *F*: Representative micturition patterns of single freely moving mice. Administration of TNFRI increased micturition volume (*G*) and decreased the frequency of small volume voids (<10 μL) (*H*). *I*: The level of TNF-α in serum. *J*: ROCK activity in bladder smooth muscle homogenates. *K*: Representative immunoblot analysis. Calm, calmodulin; GAPDH, glyceraldehyde-3-phosphate dehydrogenase. GTT value before treatment (*L*) and at 3 weeks (*M*), and 6 weeks after treatment (*N*). Data (*n* = 6 mice for each group) are representative of three different experiments and are expressed as the means ± SEM, by one-way ANOVA. **P* < 0.05, ***P* < 0.01, and ****P* < 0.001 compared with floxed control (CTR) group. #*P* < 0.05 and ##*P* < 0.01 compared with DKO nontreated control group.**

weeks) was significantly increased, but decreased at the late stage (age 20 weeks). These temporal changes in spontaneous smooth muscle activity and contractile responses to EFS, KCl, and carbachol stimulation are consistent with a compensation–decompensation progression of bladder function in this animal model of type 2 diabetes, analogous to urodynamic findings in patients with type 2 diabetes (2,30). Because all tension data were normalized for the length, width, and weight of the muscle strips, the response to stimuli reflects an inherent change in the bladder smooth muscle. Notably, we observed a parallel alteration in response to EFS and direct receptor activation by carbachol,

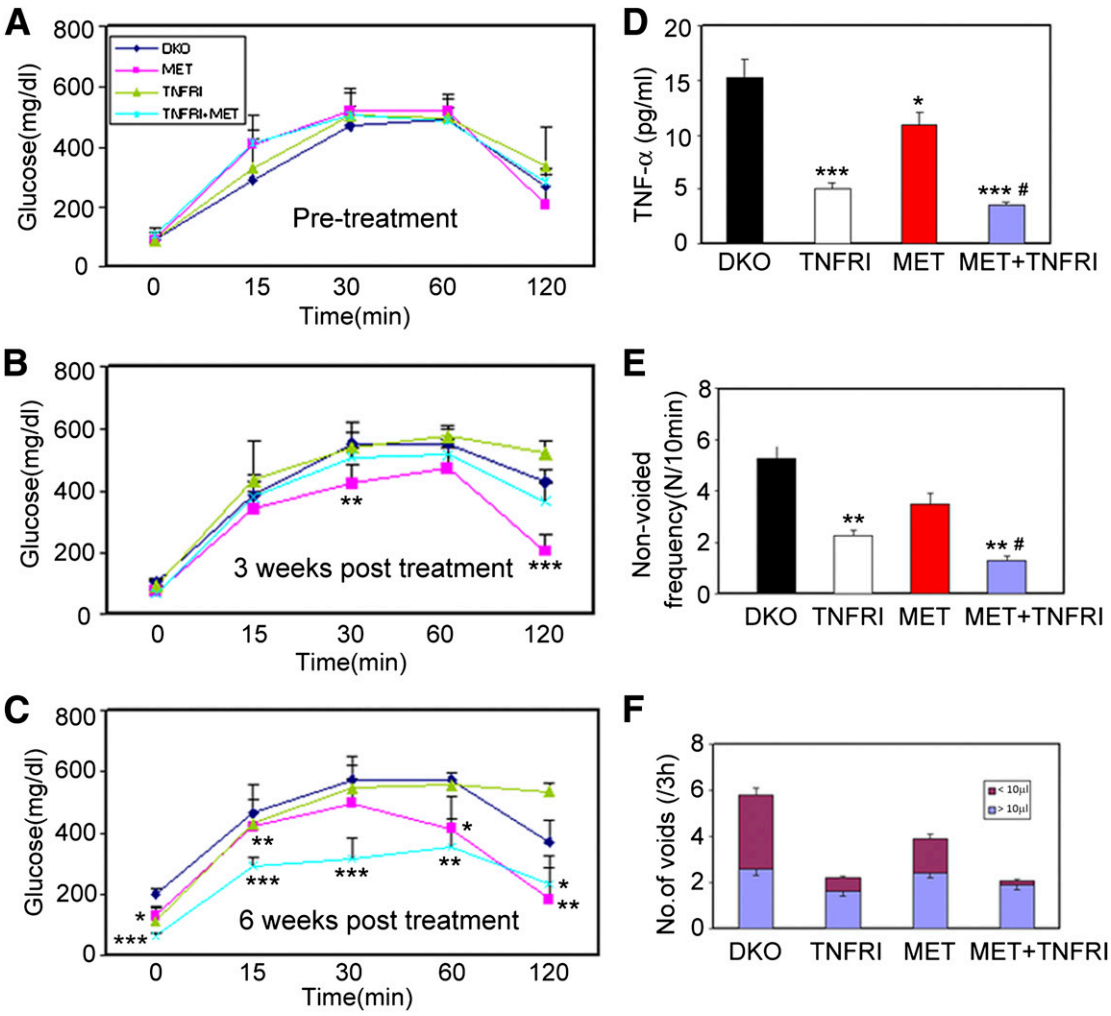


**FIG. 8. Combination of metformin (Met) and TNFRI synergistically improved the bladder dysfunction in 12-week-old DKO mice. Six-week-old animals were treated intraperitoneally with 2 mg/kg TNFRI or saline for 6 weeks, twice weekly. Metformin (2 mg/L) was supplemented in drinking water for the duration of the experiment. Control animals drank normal water. The effect of TNFRI$^{+/-}$ metformin treatment on blood glucose level of DKO animals before treatment (*A*), 3 weeks after treatment (*B*), and 6 weeks after treatment (*C*). The TNF-α level in serum (*D*), the frequency of nonvoiding contractions (*E*), and the frequency of small volume (<10 μL) voids (*F*) after 6 weeks of treatment ($n$ = 6 mice for each group). Data are representative of three different experiments and are expressed as the means ± SEM, by one-way ANOVA. *$P$ < 0.05, **$P$ < 0.01, and ***$P$ < 0.001 compared with DKO nontreated control group. #$P$ < 0.05 compared with TNFRI-treated group.**

suggesting a myogenic basis for the abnormal contraction of DKO bladder smooth muscle. However, our findings do not exclude a neuropathic change in bladder innervation that may play a role in DBD in DKO animals.

Previous studies using STZ-induced type 1 diabetes models in rats and mouse, or the Zucker type 2 diabetic and obese rat model, have shown that diabetes in these animal models is associated with increased bladder weight, prolonged duration of bladder muscle contraction, and increased residual rine volume (31). Work from Dr. Damaser's Urological Biomechanics Laboratory (Cleveland Clinic) has further shown that the voiding dysfunction was only evident in Zucker obese diabetic rats but not in Zucker nonobese diabetic rats (31). In our study, however, we did not find any statistical difference in the bladder-to-body weight ratio between DKO and age-matched control mice. We observed clear signs of bladder overactivity for the early stage (6- and 12-week-old) DKO mice, and hypoactivity in older (20-week-old) DKO animals. The different mechanism in DKO mice versus Zucker rats might cause this functional discrepancy in diabetic animal bladders. In the Zucker rat model, fibrosis of the external urethral sphincter, bladder wall edema, and vasculopathy attributed to the bladder dysfunction in the obese animals (31). In our DKO model, however, inflammation was the main finding, especially elevated TNF-α systemically and locally in the bladder, but without any identifiable gross histologic changes, changes that are more compatible with human patients with type 2 diabetes (32).

Studies have shown that diabetes-induced diuresis might contribute to the bladder dysfunction by altering the nerves and vasculature of the urinary bladder (7,9). We did not evaluate diuresis because the voiding frequency was equivalent in diabetic and nondiabetic animals and the voided volume was even reduced in DKO diabetic mice. In addition, absence of a diuretic response in our model could explain why the bladder-to-body weight ratios were not changed in our model. However, there is significant diuresis in type 1 diabetic animal models that can partly explain the bladder hypertrophy and increased bladder-to-body weight ratios (33).

The initiation of smooth muscle contractility is predominantly controlled by a calcium-dependent increase in $MLC_{20}$ phosphorylation (34). Activation of Rho A may be

of particular importance and lead to subsequent activation of Rho kinase in BSMCs (35). Here we observed that TNF-α not only promoted the contraction of BSMCs but also activated ROCK1 and ROCK2 and induced the phosphorylation of $MLC_{20}$, which suggests a close link between TNF-α and the ROCK-signaling pathway in DBD. This association was further confirmed by anti–TNF-α treatment, which not only improved bladder function but also suppressed the TNF-α level and ROCK pathway. Generally, these observations support an important role for TNF-α in DKO bladder dysfunction and indicate that TNF-α may be responsible for the observed phenotypic differences in isolated bladder tissue and in vivo.

Given that TNF-α plays a key role in the pathogenesis of DBD, anti-TNF therapy was expected to provide protection against the toxicity of TNF-α (36). Anti–TNF-α reagents significantly improved insulin resistance and reduced leukocyte adherence in retinal blood vessels of diabetic rats (37–39). In humans, however, the importance of this mechanism is much debated because limited studies of anti–TNF-α reagents have shown little or no effect on the insulin-resistant state (40). Our experimental findings match the clinical findings of Ofei et al. (40), who showed no significant alteration of hyperglycemia with anti–TNF-α treatment. However, we observed significant improvements of the parameters associated with secondary contractions of diabetes as measured by bladder function (Fig. 7). Moreover, our data further suggest that the benefit of anti–TNF-α therapy on DBD might be achieved through blockade of TNF-α–induced ROCK-MLC signaling pathway and improvement of abnormal BSMC contractility. Notably, our findings further indicate that targeted inhibition of TNF-α combined with the oral hypoglycemic agent, metformin, can synergistically improve the abnormalities associated with DBD.

In conclusion, our study provides the first demonstration that DKO mice represent a novel animal model to investigate DBD associated with type 2 diabetes. We demonstrate that the TNF-α–ROCK–pMLC pathway may represent a new target to treat patients with DBD dysfunction and provide proof of principle that pharmacologic inhibition of TNF-α can mitigate the urinary tract complications of type 2 diabetes without affecting serum glucose levels. Furthermore, the synergistic benefit of metformin and TNFRI in reversing DBD has significant clinical implications in long-term management of patients with type 2 diabetes.

## ACKNOWLEDGMENTS

This work was funded by National Institutes of Health/National Institute of Diabetes and Digestive and Kidney Diseases grant (Animal Models of Diabetic Complications Pilot & Feasibility Project, 09MCG72) and the American Urological Association/Pfizer Pharmaceutical Company competitive grants to A.F.O. No other potential conflicts of interest relevant to this article were reported.

Z.W. designed and performed research, analyzed the data, developed the animal model, and wrote the manuscript. Z.C. and M.P.S. performed research, analyzed the data, and wrote the manuscript. V.C. performed research and analyzed the data. J.L., X.X., P.G., E.G., and K.S. performed research. R.G. analyzed the data. R.M.A. analyzed the data and wrote the manuscript. M.F.W. developed the animal model. A.F.O. designed the research and wrote the manuscript. Z.W. and A.F.O. are the guarantors of this work, and as such, had full access to all the data in the study and take responsibility for the integrity of data and the accuracy of the data analysis.

## REFERENCES

1. Centers for Disease Control and Prevention. Diabetes public health resource [Internet] 2011. Available from http://www.cdc.gov/diabetes/pubs. Accessed 10 October 2011
2. Ellenberg M. Nonneurologic manifestations of diabetic neuropathy. Mt Sinai J Med 1980;47:561–567
3. Bradley WE. Diagnosis of urinary bladder dysfunction in diabetes mellitus. Ann Intern Med 1980;92:323–326
4. Lee WC, Wu HP, Tai TY, Yu HJ, Chiang PH. Investigation of urodynamic characteristics and bladder sensory function in the early stages of diabetic bladder dysfunction in women with type 2 diabetes. J Urol 2009;181:198–203
5. Daneshgari F, Moore C. Diabetic uropathy. Semin Nephrol 2006;26:182–185
6. Daneshgari F, Liu G, Birder L, Hanna-Mitchell AT, Chacko S. Diabetic bladder dysfunction: current translational knowledge. J Urol 2009;182 (Suppl.):S18–S26
7. Liu G, Li M, Vasanji A, Daneshgari F. Temporal diabetes and diuresis-induced alteration of nerves and vasculature of the urinary bladder in the rat. BJU Int 2011;107:1988–1993
8. Daneshgari F, Liu G, Imrey PB. Time dependent changes in diabetic cystopathy in rats include compensated and decompensated bladder function. J Urol 2006;176:380–386
9. Daneshgari F, Huang X, Liu G, Bena J, Saffore L, Powell CT. Temporal differences in bladder dysfunction caused by diabetes, diuresis, and treated diabetes in mice. Am J Physiol Regul Integr Comp Physiol 2006; 290:R1728–R1735
10. Dong XC, Copps KD, Guo S, et al. Inactivation of hepatic Foxo1 by insulin signaling is required for adaptive nutrient homeostasis and endocrine growth regulation. Cell Metab 2008;8:65–76
11. Cheng Z, Guo S, Copps K, et al. Foxo1 integrates insulin signaling with mitochondrial function in the liver. Nat Med 2009;15:1307–1311
12. Adam RM. Recent insights into the cell biology of bladder smooth muscle. Nephron, Exp Nephrol 2006;102:e1–e7
13. Lin X, Taguchi A, Park S, et al. Dysregulation of insulin receptor substrate 2 in beta cells and brain causes obesity and diabetes. J Clin Invest 2004; 114:908–916
14. Everaerts W, Zhen X, Ghosh D, et al. Inhibition of the cation channel TRPV4 improves bladder function in mice and rats with cyclophosphamide-induced cystitis. Proc Natl Acad Sci USA 2010;107:19084–19089
15. Gevaert T, Vriens J, Segal A, et al. Deletion of the transient receptor potential cation channel TRPV4 impairs murine bladder voiding. J Clin Invest 2007;117:3453–3462
16. Cristofaro V, Peters CA, Yalla SV, Sullivan MP. Smooth muscle caveolae differentially regulate specific agonist induced bladder contractions. Neurourol Urodyn 2007;26:71–80
17. Ramachandran A, Ranpura SA, Gong EM, Mulone M, Cannon GM Jr, Adam RM. An Akt- and Fra-1-dependent pathway mediates platelet-derived growth factor-induced expression of thrombomodulin, a novel regulator of smooth muscle cell migration. Am J Pathol 2010;177:119–131
18. Devost D, Zingg HH. Novel in vitro system for functional assessment of oxytocin action. Am J Physiol Endocrinol Metab 2007;292:E1–E6
19. Olumi AF, Grossfeld GD, Hayward SW, Carroll PR, Tlsty TD, Cunha GR. Carcinoma-associated fibroblasts direct tumor progression of initiated human prostatic epithelium. Cancer Res 1999;59:5002–5011
20. He WQ, Peng YJ, Zhang WC, et al. Myosin light chain kinase is central to smooth muscle contraction and required for gastrointestinal motility in mice. Gastroenterology 2008;135:610–620
21. Fairbank NJ, Connolly SC, Mackinnon JD, Wehry K, Deng L, Maksym GN. Airway smooth muscle cell tone amplifies contractile function in the presence of chronic cyclic strain. Am J Physiol Lung Cell Mol Physiol 2008; 295:L479–L488
22. Zhang X, Zhang L, Yang H, et al. c-Fos as a proapoptotic agent in TRAIL-induced apoptosis in prostate cancer cells. Cancer Res 2007;67:9425–9434
23. Ge R, Wang Z, Zeng Q, Xu X, Olumi AF. F-box protein 10, an NF-κB-dependent anti-apoptotic protein, regulates TRAIL-induced apoptosis through modulating c-Fos/c-FLIP pathway. Cell Death Differ 2011;18:1184–1195
24. Mong PY, Wang Q. Activation of Rho kinase isoforms in lung endothelial cells during inflammation. J Immunol 2009;182:2385–2394
25. Ghosh K, Thodeti CK, Dudley AC, Mammoto A, Klagsbrun M, Ingber DE. Tumor-derived endothelial cells exhibit aberrant Rho-mediated mechanosensing and abnormal angiogenesis in vitro. Proc Natl Acad Sci USA 2008;105: 11305–11310

26. Liu G, Daneshgari F. Alterations in neurogenically mediated contractile responses of urinary bladder in rats with diabetes. Am J Physiol Renal Physiol 2005;288:F1220–F1226
27. McCloskey KD, Anderson UA, Davidson RA, Bayguinov YR, Sanders KM, Ward SM. Comparison of mechanical and electrical activity and interstitial cells of Cajal in urinary bladders from wild-type and W/Wv mice. Br J Pharmacol 2009;156:273–283
28. Brownlee M. Biochemistry and molecular cell biology of diabetic complications. Nature 2001;414:813–820
29. Andersson KE, Arner A. Urinary bladder contraction and relaxation: physiology and pathophysiology. Physiol Rev 2004;84:935–986
30. Frimodt-Møller C. Diabetic cystopathy: epidemiology and related disorders. Ann Intern Med 1980;92:318–321
31. Gasbarro G, Lin DL, Vurbic D, et al. Voiding function in obese and type 2 diabetic female rats. Am J Physiol Renal Physiol 2010;298:F72–F77
32. Wellen KE, Hotamisligil GS. Inflammation, stress, and diabetes. J Clin Invest 2005;115:1111–1119
33. Liu G, Daneshgari F. Temporal diabetes- and diuresis-induced remodeling of the urinary bladder in the rat. Am J Physiol Regul Integr Comp Physiol 2006;291:R837–R843
34. Sellers JR, Homsher E. A giant step for myosin. Curr Biol 1991;1:347–349
35. Matsui T, Amano M, Yamamoto T, et al. Rho-associated kinase, a novel serine/threonine kinase, as a putative target for small GTP binding protein Rho. EMBO J 1996;15:2208–2216
36. Saltiel AR, Kahn CR. Insulin signalling and the regulation of glucose and lipid metabolism. Nature 2001;414:799–806
37. Kern TS. Contributions of inflammatory processes to the development of the early stages of diabetic retinopathy. Exp Diabetes Res 2007;2007:95103
38. Joussen AM, Poulaki V, Mitsiades N, et al. Nonsteroidal anti-inflammatory drugs prevent early diabetic retinopathy via TNF-alpha suppression. FASEB J 2002;16:438–440
39. Ventre J, Doebber T, Wu M, et al. Targeted disruption of the tumor necrosis factor-alpha gene: metabolic consequences in obese and nonobese mice. Diabetes 1997;46:1526–1531
40. Ofei F, Hurel S, Newkirk J, Sopwith M, Taylor R. Effects of an engineered human anti-TNF-alpha antibody (CDP571) on insulin sensitivity and glycemic control in patients with NIDDM. Diabetes 1996;45:881–885